

## Ringling phenomenon in coupled cavities: Application to modal coupling in whispering-gallery-mode resonators

Stéphane Trebaol, Yannick Dumeige,\* and Patrice Féron

*ENSSAT-FOTON (CNRS-UMR 6082), Université de Rennes 1, F-22300 Lannion, France*

(Received 5 September 2009; published 22 April 2010)

We present a simple model to describe the transient response of two coupled resonators probed by a monochromatic wave whose frequency is rapidly swept across the resonances with respect to their characteristic photon lifetimes. The model is applied to analyze the dynamic behavior of the modal coupling between two degenerate resonances of the same cavity. In particular, this can be used to describe the coupling of counterpropagating whispering gallery modes (WGMs) by Rayleigh scattering. The theory is successfully compared to experiments carried out in silica microspheres. These results show that this ringdown technique can be extended to accurately measure linear properties and frequency splittings of high-quality factor WGM microresonators.

DOI: [10.1103/PhysRevA.81.043828](https://doi.org/10.1103/PhysRevA.81.043828)

PACS number(s): 42.60.Da, 42.25.Hz, 42.25.Fx, 42.55.Sa

### I. INTRODUCTION

Optical high-quality-factor ( $Q$ ) microcavities are of great interest for applications in different fields such as optoelectronics, metrology or fundamental physics [1–3]. They can be used, for instance, for optical filtering, all-optical switching [4], low-threshold nonlinear optics [5,6], narrow linewidth laser applications [7,8], all-optical buffering [9,10], biosensing [11], and quantum information processing or cavity quantum electrodynamics [12]. The coupling of optical microresonators offers supplementary degrees of freedom and can also be used for the same purposes as single resonators with additional functionalities. Using coupled microrings, high order optical filtering can be achieved [13] and all-optical regeneration could be miniaturized [14]. The coupling of nonlinear microrings leads to the implementation of new phase-matching schemes [15–17] for frequency conversion or to the reduction of multistability threshold [18]. It has been shown that the dispersion high orders of coupled resonators optical waveguides [19,20] can be canceled by optimizing the coupling between microresonators. This could have potential applications in optical delay lines integration [21,22].

When a single high- $Q$  resonator is excited using an input field whose frequency is linearly swept across the resonance with a duration shorter than the cavity lifetime, its transmission response shows oscillations [23,24]. It has already been demonstrated that this ringing phenomenon can be used to accurately measure the resonator characteristics for passive Fabry-Pérot resonators [25,26]. In the case of microresonators this “self-homodyne method” has been used to measure  $Q$  factors greater than  $10^{10}$  without a highly stabilized laser [27,28]. The method can also be extended in order to measure thoroughly the coupling regime and even the external gain in the case of active resonators [29] and to take into account microresonator thermal properties [30]. Finally, it has been shown that ringing of a single resonator description can also be applied for two coupled resonators under a particular coupling

configuration where one of the resonator acts as a purely dispersive medium [31,32].

In this paper we present, in the general case, a simple model for the calculation of the transient linear response of coupled cavities excited by a field whose carrier frequency is linearly swept in time. We also experimentally demonstrate, for the first time in coupled resonators, the ringing effect coming from this linear frequency sweeping. We also show that the comparison of experiment results with calculations allows the linear parameters and coupling characteristics of the coupled cavity system to be inferred. The experimental results are obtained in a single whispering gallery mode (WGM) microsphere where Rayleigh backscattering couples the two frequency degenerated clockwise (CW) and counterclockwise (CCW) modes [33,34]. This phenomenon often referred to as modal coupling [35] has already been studied in the stationary regime and all the authors have reported a resonance splitting in the transmission spectrum coming from the coupling of the two CW and CCW modes [7,33,36]. Weiss *et al.* [33] have also reported time domain observation of the beat note of the two split resonance frequencies using a frequency locked laser. Modal coupling must be well analyzed not only to accurately characterize bare WGM resonators [37,38] but also to investigate the spectral properties of WGM coupled to single subwavelength scatterer or emitter [39–41]. From an application point of view, Rayleigh backscattering in high- $Q$  resonators has been used as optical feedback for narrow linewidth laser diode or Erbium doped fiber laser [7,43,44].

The paper is organized as follows. In Sec. II we present a simple model for ringing phenomenon in coupled cavities in the general case. The model is deeply developed in the case of modal coupling in a single traveling wave resonator. Sec. III is devoted to the experimental validation of the proposed model. We have used high- $Q$  silica microsphere where Rayleigh scattering can be experimentally observed. The comparison between theory and experiments is carried out using a numerical procedure. We check the validity and the robustness of our method using the stationary regime comparison and different coupling regimes. Finally we discuss the interests of the proposed method.

\*yannick.dumeige@enssat.fr

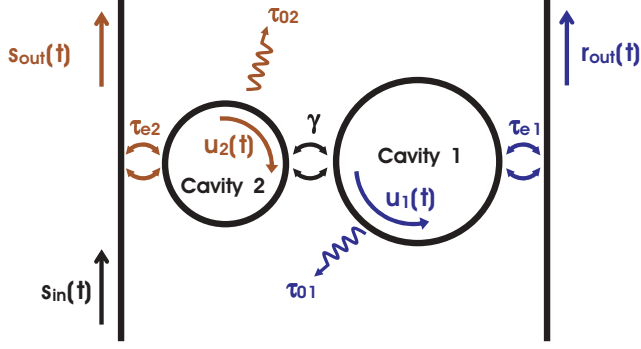


FIG. 1. (Color online) Schematic representation of two single-mode coupled cavities. Cavity 2 is coupled to the input/output port whereas cavity 1 is only coupled to one output port.

## II. THEORETICAL DESCRIPTION OF RINGING EFFECT IN COUPLED CAVITIES

### A. General formalism

The generic system is described in Fig. 1. It consists of two coupled cavities of resonant angular frequencies  $\omega_1$  and  $\omega_2$ . The mutual coupling of the two cavities is characterized by a lifetime  $\gamma$ . The coupling with the access lines are also described by two lifetimes  $\tau_{e1}$  and  $\tau_{e2}$ .  $\tau_{o1}$  and  $\tau_{o2}$  are the intrinsic lifetimes of the two cavities. We assume for simplicity that the input signal  $s_{in}(t) = s_0 e^{j\varphi(t)}$  is directly coupled to cavity 2. The mode amplitude evolutions for two cavities are given by integrating the following equations [33,35,45]:

$$\begin{aligned} \dot{u}_1 &= a_1 u_1(t) + b u_2(t) \\ \dot{u}_2 &= b u_1(t) + a_2 u_2(t) + f(t), \end{aligned} \quad (1)$$

where for  $i \in \{1, 2\}$  we have  $a_i = j\omega_i - \frac{1}{\tau_i}$ ,  $\tau_i^{-1} = \tau_{oi}^{-1} + \tau_{ei}^{-1}$ ,  $b = \frac{j}{2\gamma}$ , and  $f(t) = \sqrt{\frac{2}{\tau_{e2}}} s_{in}(t)$ . The outputs are calculated from the mode amplitude expressions:

$$\begin{aligned} s_{out}(t) &= -s_{in}(t) + \sqrt{\frac{2}{\tau_{e2}}} u_2(t) \\ r_{out}(t) &= \sqrt{\frac{2}{\tau_{e1}}} u_1(t). \end{aligned} \quad (2)$$

It is now possible to define the amplitude transmission coefficient  $x = s_{out}/s_{in}$  and the amplitude reflection coefficient  $y = r_{out}/s_{in}$  which are related to the intensity transmission ( $T$ ) and reflection ( $R$ ) coefficients by  $T = |x|^2$  and  $R = |y|^2$ . In order to obtain the solutions of system (1), we can write its eigenvalues:

$$\Lambda_{\pm} = j\omega_M \pm \frac{\sqrt{\delta^2 + 4b^2}}{2}, \quad (3)$$

where  $j\omega_M = \frac{a_1 + a_2}{2}$  and  $\delta = a_2 - a_1$ . Thus, the differential system (1) can be solved by using the new variables:

$$u_{\pm}(t) = \frac{-\delta \pm \sqrt{\delta^2 + 4b^2}}{2b} u_1(t) + u_2(t), \quad (4)$$

and by integrating

$$\frac{du_{\pm}}{dt} = \Lambda_{\pm} u_{\pm} + f(t). \quad (5)$$

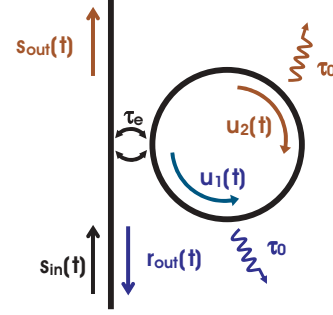


FIG. 2. (Color online) Schematic sketch of modal coupling due to enhanced backscattering in a single resonator.

The response of the coupled cavities can be calculated for any arbitrary input field  $f(t)$ . In particular, using an input phase  $\varphi(t) = \omega t$  it is possible to obtain the stationary response of the system at the angular frequency  $\omega$ . In the next section we will apply this general formalism to the particular case of modal coupling.

### B. Application to modal coupling

Numerous authors have reported the observation of split resonances in the transmission spectrum of high-finesse traveling wave resonators [7,33,36]. This resonant frequency splitting is generally attributed to the coupling of two degenerate modes propagating in the opposite direction [33]. In our physical picture (see Fig. 2), the CW mode is modeled by  $u_2$  and the CCW mode by  $u_1$ . The origin of this coupling can come from enhanced Rayleigh backscattering or nanoscale isolated scatterers [40]. The general formalism proposed in the previous section can be applied assuming the following simplifications:  $\omega_1 = \omega_2 = \omega_0$ ,  $\tau_{o1} = \tau_{o2} = \tau_0$ ,  $\tau_{e1} = \tau_{e2} = \tau_e$ ,  $\tau_1 = \tau_2 = \tau$ , and thus  $a_1 = a_2 = a$ . Consequently, the system (1) is also simplified and we then obtain:  $\omega_M = \omega_0$ ,  $\delta = 0$ ,  $\Lambda_{\pm} = a \pm b$ . Consequently  $u_{\pm}(t) = u_2(t) \pm u_1(t)$  and Eq. (5) reduces to

$$\frac{du_{\pm}}{dt} = (a \pm b)u_{\pm}(t) + f(t). \quad (6)$$

The mode amplitude  $u_1(t)$  and  $u_2(t)$  are easily calculated noticing that  $u_2 = (u_+ + u_-)/2$  and  $u_1 = (u_+ - u_-)/2$ .

#### 1. Stationary behavior

First, assuming a stationary excitation, we have  $\varphi(t) = \omega t$  and the solutions of Eq. (6) are given by

$$u_{\pm}(t) = \sqrt{\frac{2}{\tau_e}} \frac{s_0 e^{j\omega t}}{j\omega - a \mp b}. \quad (7)$$

As proposed in Ref. [34], the amplitude transmission coefficient can be written:

$$x(\omega) = \frac{b^2 - (j\omega - a)^2 + 2(j\omega - a)/\tau_e}{(j\omega - a)^2 - b^2}, \quad (8)$$

whereas the amplitude reflection coefficient can be obtained by

$$y(\omega) = \frac{2b/\tau_e}{(j\omega - a)^2 - b^2}. \quad (9)$$

The inspection of the denominators of Eq. (9) shows that if  $\gamma < \tau/2$  the coupled system has two new resonant frequencies separated by a quantity:

$$2\delta_C = \frac{1}{2\pi\gamma} \sqrt{1 - \left(\frac{2\gamma}{\tau}\right)^2}, \quad (10)$$

which constitutes the modal coupling splitting frequency experimentally observed in the reflected signal [38].

## 2. Frequency sweeping

Now we consider a linear frequency sweeping with an angular frequency speed  $V_S$ , thus the phase of the input signal can be now written:

$$\varphi(t) = \omega_i t + \frac{V_S}{2} t^2, \quad (11)$$

where  $\omega_i$  is the frequency at  $t = 0$  since the instantaneous angular frequency reads  $\dot{\varphi}(t) = \omega_i + V_S t$ . Solving Eq. (6) we find

$$u_{\pm}(t) = \left( A_{\pm} + \int_0^t f(t') e^{-(a \pm b)t'} dt' \right) e^{(a \pm b)t}, \quad (12)$$

where  $A_{\pm}$  is obtained using the stationary solution [given in Eq. (7)] for an angular frequency  $\omega_i$ :

$$A_{\pm} = \sqrt{\frac{2}{\tau_e}} \frac{s_0}{j\omega_i - a \mp b}, \quad (13)$$

and

$$\int_0^t f(t') e^{-(a \pm b)t'} dt' = g_{\pm}(t) - g_{\pm}(0), \quad (14)$$

where  $g_{\pm}(t)$  can be analytically expressed using the complex error function  $\text{erf}(z)$  with  $z \in \mathbb{C}$ :

$$g_{\pm}(t) = -s_0 \sqrt{\frac{j\pi}{\tau_e V_S}} \exp\left(\frac{j(a \pm b - j\omega_i)^2}{2V_S}\right) \times \text{erf}\left(-\frac{j(a \pm b) + V_S t + \omega_i}{\sqrt{2jV_S}}\right). \quad (15)$$

As it has already been reported in Ref. [31] for single resonators, the present method based on coupled mode theory is more convenient to describe ringing phenomenon than the summation of partial fields. In the case of coupled resonators the use of partial fields would be much more fastidious than the proposed method.

## C. Numerical simulations

The calculation procedure presented in the previous section is used to simulate the coupled cavity ringing phenomenon for a cavity under modal coupling in different examples. As it has already been proposed in Ref. [35] we define  $\Gamma = \tau_0/(2\gamma)$  and  $K = \tau_0/\tau_e$  to characterize the coupling and the cavity quality. This definition allows the critical coupling  $x(\omega_0) = 0$  to be defined by  $K = \sqrt{1 + \Gamma^2}$  [34,35]. All the frequency scanning speeds  $\tilde{V}_S = V_S/(2\pi)$  are compared to the normalized frequency speed  $\tilde{V}_0 = 2/(\pi\tau^2)$  which corresponds to one resonance of frequency width  $1/(\pi\tau)$  scanned during the ringdown time  $\tau/2$  [29].

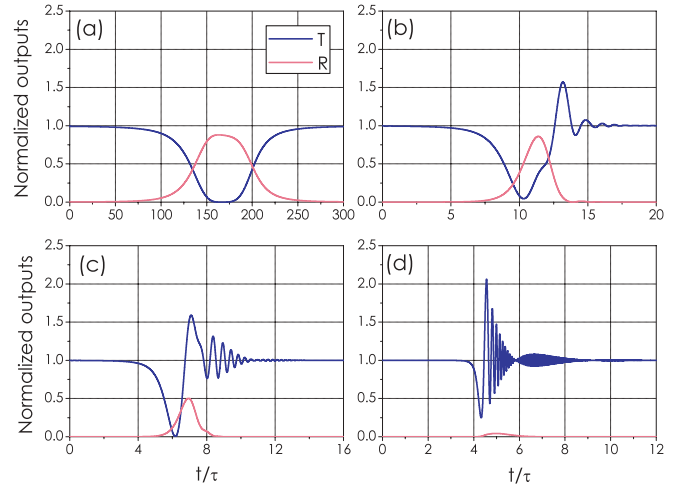


FIG. 3. (Color online) Variations of the transmission ( $T$ ) and the reflectivity ( $R$ ) for a cavity under modal coupling in the case of  $\Gamma = 15$  and critical coupling ( $K = \sqrt{1 + \Gamma^2}$ ). The input signal is linearly swept with several sweeping speeds: (a)  $\tilde{V}_S = 0.01\tilde{V}_0$ , (b)  $\tilde{V}_S = 0.3\tilde{V}_0$ , (c)  $\tilde{V}_S = \tilde{V}_0$ , and (d)  $\tilde{V}_S = 12\tilde{V}_0$ . The abscissas are normalized for  $\tau$ .

### 1. Critical coupling

We start by showing in Fig. 3 the ringing effect in the case of the critical coupling in the particular case of  $\Gamma = 15$  arbitrarily chosen. For low scanning speeds (here  $\tilde{V}_S = 0.01\tilde{V}_0$ ) we find the stationary response of the system as represented in Fig. 3(a). The transmission drops to zero at resonance and the reflection is maximal [35]. When the scanning speed is increased as is the case in Figs. 3(b) and 3(c), ringing oscillations appear as is the case for single resonators [25]. For high scanning speed ( $\tilde{V}_S = 12\tilde{V}_0$ ) it is possible to distinguish a modulation of the oscillation amplitude coming from the beating of the split frequencies [Fig. 3(d)].

### 2. $\Gamma > 1$ and $K < 1$

We now consider a case where we have chosen  $\Gamma = 7$  and  $K = 1/3$  (see Fig. 4). The quasistationary ( $\tilde{V}_S = 0.01\tilde{V}_0$ ) response given in Fig. 4(a) shows two resonances with an associated transmission greater than 50%. When the sweeping speed ( $\tilde{V}_S = 0.3\tilde{V}_0$ ) is increased, we obtain two transient profiles looking as the response of an undercoupled single resonator in good agreement with the value of  $K < 1$  [Fig. 4(b)]. For higher sweeping speeds shown in Figs. 4(c) and 4(d), the beating of the two resonance frequencies is much more visible than in the critical case.

### 3. $\Gamma \gg 1$ and $K > 1$

For the last example shown in Fig. 5 we have chosen  $\Gamma = 50$  and  $K = 10$ . For  $\tilde{V}_S = 0.01\tilde{V}_0$ , the quasistationary response of Fig. 5(a) consists of two dips with zero transmission. Since  $K > 1$ , for  $\tilde{V}_S = 0.3\tilde{V}_0$  we obtain the transient response of two overcoupled single resonators [Fig. 5(b)]. For high sweeping speeds as represented in Figs. 5(c) and 5(d) we observe a strong beating between the two resonant frequencies.

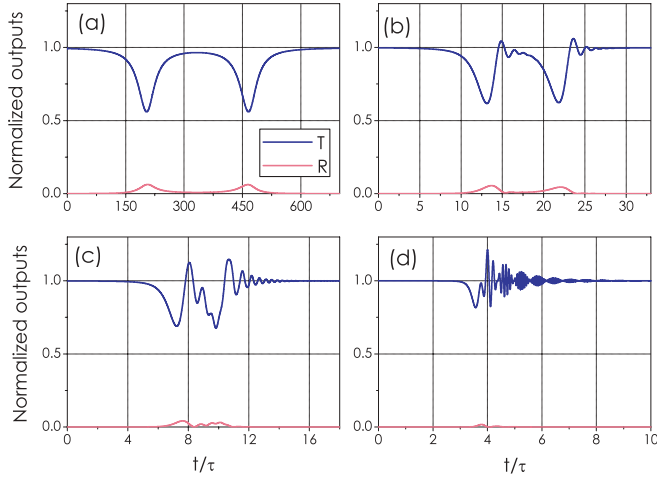


FIG. 4. (Color online) Variations of the transmission ( $T$ ) and the reflectivity ( $R$ ) for a cavity under modal coupling in the case of  $\Gamma = 7$  and  $K = 1/3$ . The input signal is linearly swept with several sweeping speeds: (a)  $\tilde{V}_S = 0.01\tilde{V}_0$ , (b)  $\tilde{V}_S = 0.3\tilde{V}_0$ , (c)  $\tilde{V}_S = \tilde{V}_0$ , and (d)  $\tilde{V}_S = 12\tilde{V}_0$ . The abscissas are normalized for  $\tau$ .

### III. EXPERIMENTAL VALIDATION USING SILICA MICROSPHERES

In this section we test the simple model previously developed using a silica microsphere-based system. As is the case for single resonators, we will show that it is possible to infer, from theory and experiment comparisons, the value of  $\tau_e$ ,  $\tau_0$ , and  $\tilde{V}_S$  from time domain measurements. In the present case we will show that we can also obtain the value of  $\gamma$ . The system consists of a microsphere coupled to a fiber taper by evanescent waves [46]. A tuning of the gap between the sphere and the taper allows the coupling configuration to be modified.

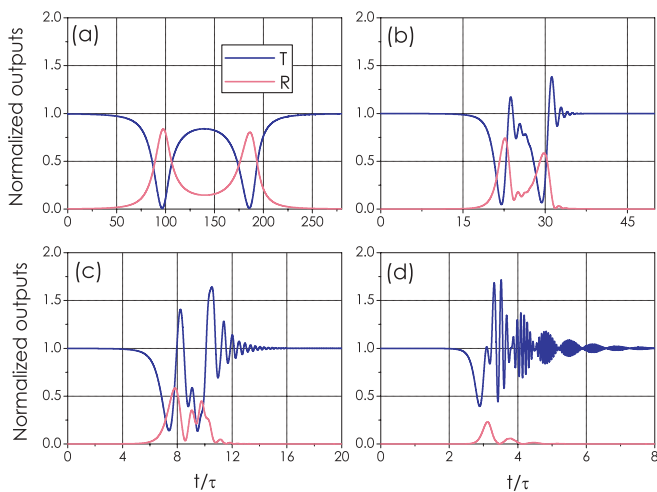


FIG. 5. (Color online) Variations of the transmission ( $T$ ) and the reflectivity ( $R$ ) for a cavity under modal coupling in the case of  $\Gamma = 50$  and  $K = 10$ . The input signal is linearly swept with several sweeping speeds: (a)  $\tilde{V}_S = 0.025\tilde{V}_0$ , (b)  $\tilde{V}_S = 0.3\tilde{V}_0$ , (c)  $\tilde{V}_S = \tilde{V}_0$ , and (d)  $\tilde{V}_S = 12\tilde{V}_0$ . The abscissas are normalized for  $\tau$ .

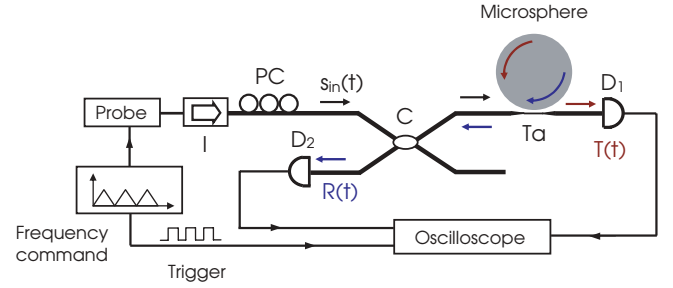


FIG. 6. (Color online) Experimental setup used to test silica microspheres. The probe is a tunable 1550-nm laser diode (linewidth 150 kHz) whose central frequency is linearly swept with a controllable period. I, optical isolator; PC, polarization controller; C, 3dB coupler; Ta, tapered fiber.  $D_1$  and  $D_2$  are two optical detectors whose bandwidth is around 10 MHz.

#### A. Experimental setup and method

Figure 6 represents the microsphere system we used in the experiments. The probe signal is a continuously tunable narrow line ( $\approx 150$  kHz) external cavity laser diode. The frequency of the probe is almost linearly swept using an electrical waveform generator. Depending on the period of the waveform we can obtain either a slow or a fast sweeping of the frequency. The slow sweeping gives us the stationary response of the microresonator. The fast scanning allows the transient response to be obtained. The diameter of the tapered fiber is reduced to  $4 \mu\text{m}$ . We have tested different spheres with diameters  $D$  between  $80$  and  $120 \mu\text{m}$ . The spheres are fabricated by melting the tip of silica rods using a fiber splicer. The probe whose wavelength is chosen around  $\lambda = 1550$  nm is coupled into the sphere using the taper which also allows the transmission and reflection signals to be extracted. The outcoupled signals from the sphere are sent to two photodetectors:  $D_1$  is used to measure  $T(t)$  and  $D_2$  to obtain  $R(t)$ . The transmission  $T(t)$  is normalized using the off-resonance value. Then we are able to obtain the experimental time domain variations of the transmission  $T_{\text{mes}}$ , which was compared to the theoretical value  $T_{\text{theo}}$  by using the least square method:

$$\sigma^2(\tau_0, \tau_e, V_S, \gamma) = \sum_{i=1}^N [T_{\text{mes},i} - T_{\text{theo},i}(\tau_0, \tau_e, V_S, \gamma)]^2, \quad (16)$$

where  $N$  is the number of time domain sampling points. The value of  $\sigma^2$  is minimized by automatically changing the value of  $\tau_0$ ,  $\tau_e$ ,  $V_S$ , and  $\gamma$  to obtain the best fit [29].

#### B. Experimental results

##### 1. Simultaneous measurement of $T$ and $R$

First we check the consistency between the transmission and the reflection signals. In this experiment we used a  $D = 120 \mu\text{m}$  microsphere. For two given split resonances, we have measured the time domain variations of the transmission signal and have fitted it using the method previously described (see Fig. 7). With these parameters we have checked that we were able to simultaneously fit the reflection signal only adjusting artificially the amplitude level which strongly depends on the taper losses and photodiode  $D_2$  sensitivity. We can observe a very good quantitative agreement between calculations and

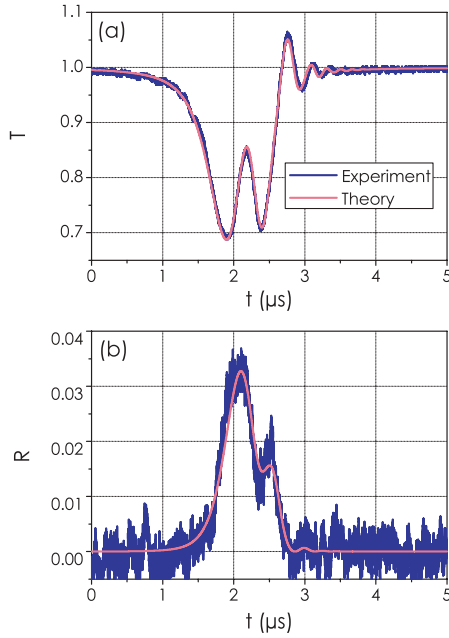


FIG. 7. (Color online) Transmission (a) and reflection (b) signals for a  $D = 120 \mu\text{m}$  microsphere. From the calculations we inferred the following values:  $\tau_0 = 267 \text{ ns}$ ,  $\tau_e = 1309 \text{ ns}$ ,  $\tilde{V}_S = 4.47 \text{ MHz}/\mu\text{s}$ , and  $1/(2\pi\gamma) = 2.38 \text{ MHz}$ .

experiments for the two signals. We can notice that the reflected signal is strongly resonant which insures that it comes from the resonator itself instead of back-reflection in any other part of our experimental setup.

## 2. Comparison to the stationary regime

In a second set of experiments we have compared the parameters inferred from time domain experiments obtained with a fast scanning of the frequency ( $\tilde{V}_S > 3 \text{ MHz}/\mu\text{s}$ ) to stationary results obtained using a slow sweeping of the frequency ( $\tilde{V}_S \approx 0.5 \text{ MHz}/\mu\text{s}$ ). Figure 8(a) represents the transient response of a split resonance observed with a  $D = 110 \mu\text{m}$  microsphere and Fig. 8(b) is the stationary response of the same split resonances. The theoretical calculations are carried out as follows: from the dynamic experiment we obtained  $\tau_0$ ,  $\tau_e$ , and  $\gamma$ ; using this set of parameters we calculate the expected stationary response and we compare it with the experimental data. Since it is difficult to accurately measure the frequency sweeping speed in the slow scanning regime, we used  $\gamma$  to calibrate the frequency axis. Note that we report here the better stationary result we have obtained. Indeed, in most of the cases we had to adjust the value of  $\tau_e$  to reach a good agreement between fast and slow sweeping experiments. Nevertheless the agreement was always satisfying since the intrinsic values  $\tau_0$  and  $\gamma$  were consistent between dynamic and stationary experiments. The discrepancy for  $\tau_e$  must come from the taper position fluctuations in time.

## 3. Influence of the coupling efficiency

We have also tested the validity of the method by recording several transient responses for the same split resonances only varying the coupling strength. The experiments are carried

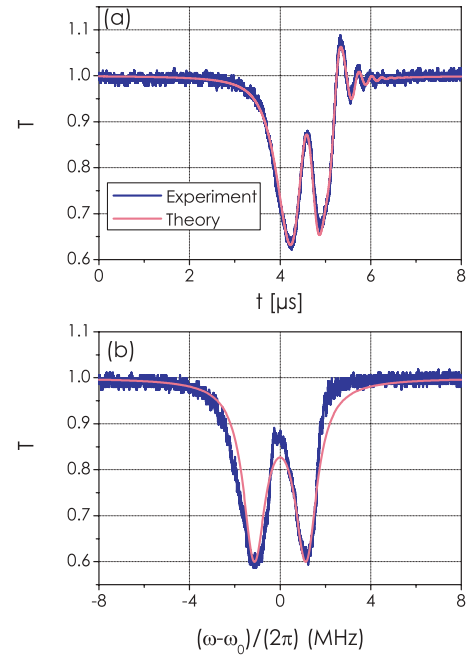


FIG. 8. (Color online) Fast (a) and slow (b) scanning experiments for a  $D = 110 \mu\text{m}$  microsphere. From the calculations given in (a) we inferred the following values:  $\tau_0 = 338 \text{ ns}$ ,  $\tau_e = 1243 \text{ ns}$ ,  $\tilde{V}_S = 3.15 \text{ MHz}/\mu\text{s}$ , and  $1/(2\pi\gamma) = 2.26 \text{ MHz}$ . These values are used to calculate the theoretical stationary response given in (b).

out by slightly changing the gap between the taper and the sphere of diameter  $D = 110 \mu\text{m}$ . The corresponding results are given in Fig. 9. For three positions indexed in Fig. 9 by (a), (b), and (c) we give the inferred linear parameters ( $\tau_0$ ,  $\tau_e$ ,  $V_S$ , and  $\gamma$ ) in Table I. From position (a) to position (c) the taper is brought closer to the sphere and thus the coupling is increased which is in good agreement with the results given in Table I. Indeed, the numerical procedure gives almost the same values of  $\tau_0$  and  $\gamma$  which intrinsically characterize the studied resonance. The sweeping speed is also constant as it is also found from the experimental measurements. On the other hand, the least-square method gives a decreasing  $\tau_e$  which shows that the coupling increases.

## 4. Supplementary experiments

Still using the sphere with a diameter  $D = 120 \mu\text{m}$  but for increased input powers we observed some thermal effects which lead to a drift of the resonance for a given frequency sweeping [27]. If the frequency sweeping is carried out in the same direction as the thermal drift, a resonance broadening is observed. For the opposite frequency scanning, since the

TABLE I. Inferred linear parameters for different taper relative positions. Positions (a), (b), and (c) are those discussed in Fig. 9.

Taper position	$\tau_0$	$\tau_e$	$1/(2\pi\gamma)$	$\tilde{V}_S$
(a)	308 ns	7996 ns	1.51 MHz	4.81 MHz/ $\mu\text{s}$
(b)	334 ns	5649 ns	1.52 MHz	4.71 MHz/ $\mu\text{s}$
(c)	318 ns	2286 ns	1.45 MHz	4.88 MHz/ $\mu\text{s}$

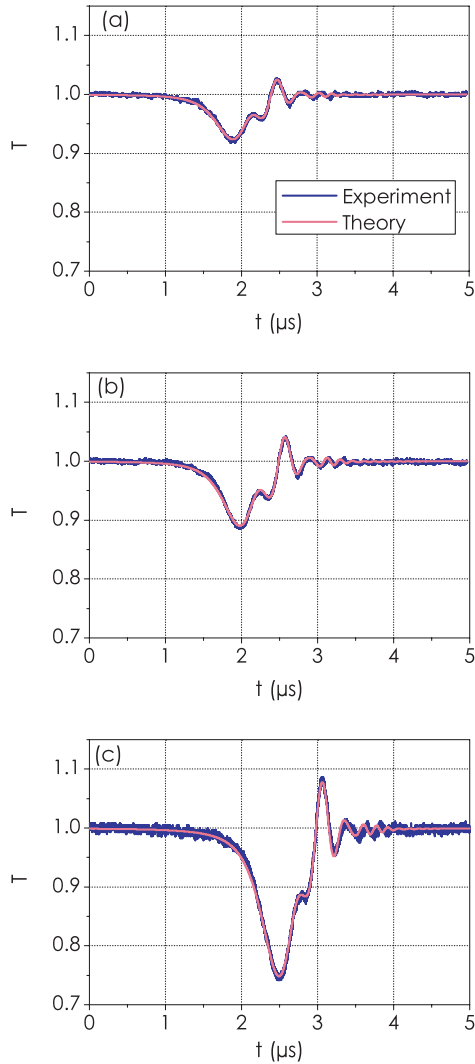


FIG. 9. (Color online) Temporal profile of the transmission for the same split resonance of a  $D = 110 \mu\text{m}$  microsphere. From (a) to (c) the gap between the taper and the sphere decreased and thus the coupling increased. The parameters obtained using the numerical procedure are given in Table I.

thermal effect shifts the resonance in the opposite way than the frequency sweeping the resonance looks narrower than it is [27,47]. With our method this last case may be analyzed assuming that the thermal effect only increased the apparent sweeping speed. The results are shown in Fig. 10. We observe much more oscillations than in the previous cases which show that for almost the same sphere quality factor (here we have  $\tau_0 = 232 \text{ ns}$ ) we have carried out a faster frequency sweeping across the resonance (with almost the same sweeping speed of the laser frequency). This is confirmed by the numerical procedure which gives a greater sweeping speed  $\tilde{V}_S = 19.5 \text{ MHz}/\mu\text{s}$ . We have also tested another microsphere sizes. For  $D = 80 \mu\text{m}$  we have easily found some more split resonances (this will be discussed later in Sec. III B5). Figure 11 is an example of a typical experimental result for a small sphere. The numerical procedure gives a frequency splitting around 4.5 MHz. This last result shows the

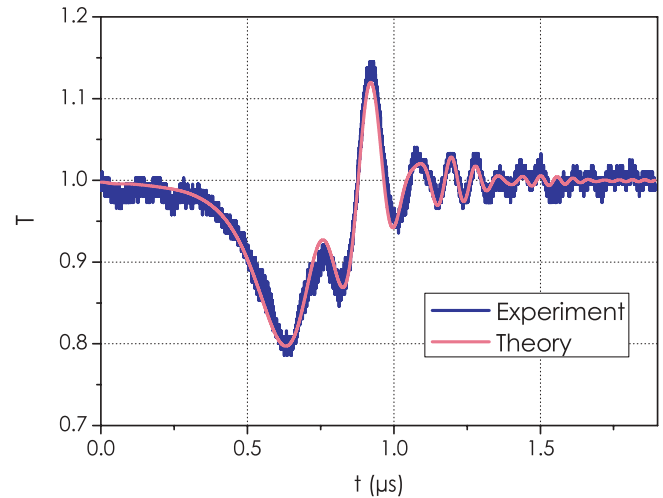


FIG. 10. (Color online) Temporal profile of the transmission of a  $D = 120 \mu\text{m}$  microsphere in the case where we observed thermal effect.  $\tau_0 = 232 \text{ ns}$ ,  $\tau_e = 1606 \text{ ns}$ ,  $\tilde{V}_S = 19.5 \text{ MHz}/\mu\text{s}$ , and  $1/(2\pi\gamma) = 3.1 \text{ MHz}$ .

potentiality of the method even in the case of more spectrally separated resonances.

### 5. Discussion

The time domain calculations are in good agreement with both transmission and reflection experimental results. The measurement procedure based on numerical fitting have been checked in the stationary regime. Our experimental method allows all the linear parameters  $\tau_0$ ,  $\tau_e$ , and  $\gamma$  to be obtained in one set of measurement. We have also checked that the numerical procedure gives relevant results when only the coupling configuration is changed. In this subsection we compare experimentally obtained frequency splittings and  $Q$ -factor values to theoretical predictions and to other author results.

(a) *Frequency splitting.* First we check that the frequency splittings measured in this work are consistent with Rayleigh

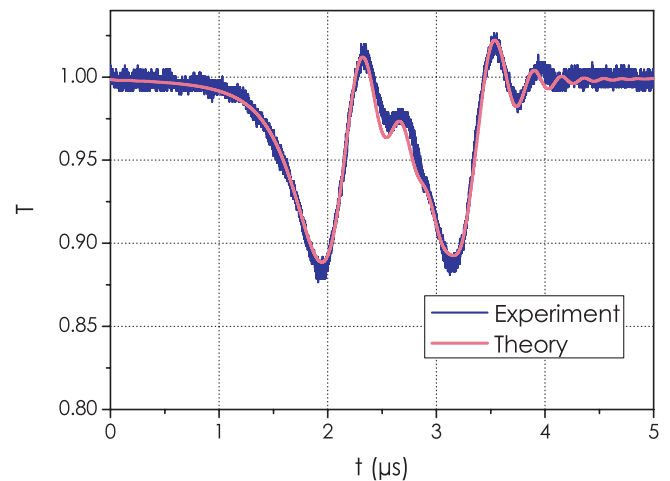


FIG. 11. (Color online) Example of a time domain profile of the transmission of a  $D = 80 \mu\text{m}$  microsphere.  $\tau_0 = 282 \text{ ns}$ ,  $\tau_e = 3829 \text{ ns}$ ,  $\tilde{V}_S = 3.7 \text{ MHz}/\mu\text{s}$ , and  $1/(2\pi\gamma) = 4.49 \text{ MHz}$ .

TABLE II. Structural parameters and associated theoretical values of the frequency splitting for the studied microspheres.

$D$	80 $\mu\text{m}$	110 $\mu\text{m}$	120 $\mu\text{m}$
$\ell$	235	323	353
$\mathcal{V}$	2070 $\mu\text{m}^3$	3720 $\mu\text{m}^3$	4360 $\mu\text{m}^3$
$1/(2\pi\gamma)$	6.0 MHz	4.5 MHz	4.1 MHz

scattering. It has been established that [33]

$$\frac{1}{2\pi\gamma} = \frac{c}{\lambda} \sqrt{\frac{\rho_{sc}\bar{\alpha}^2}{\mathcal{V}}}, \quad (17)$$

where  $\rho_{sc}$  is the scatterer number density,  $\bar{\alpha}$  their average linear polarizability, and  $\mathcal{V}$  the WGM volume. Assuming WGM with a radial order  $n = 1$ , angular and azimuthal numbers ( $\ell, m$ ) [49,50] the mode volume can be written [2,27]:

$$\mathcal{V} = 3.4\pi^{3/2} \left( \frac{\lambda}{2\pi N} \right)^3 \ell^{11/6} \sqrt{2(\ell - m) + 1}. \quad (18)$$

With  $\ell \approx \pi DN/\lambda$ , a sphere refractive index  $N \approx 1.45$  and assuming  $m = \ell$  we obtain the  $\mathcal{V}$  values given in Table II for the microsphere diameters we used. Considering  $\rho_{sc}\bar{\alpha}^2 = 2 \times 10^{-12} \mu\text{m}^3$  for silica [48] we obtain maximal values for the frequency splitting between 4.1 MHz and 6.0 MHz (see Table II) in good qualitative agreement with our experimental results.

Note that we found the largest splitting in the smallest sphere conforming to Eqs. (17) and (18). The lowest values obtained in the present work must correspond to values of  $m$  such as  $\ell > m$ . Indeed, in this case, the mode volume increases and thus the frequency splitting decreases.

(b) *Q factors.* By analogy with a single resonance, we can define an intrinsic  $Q$  factor by  $Q_0 = \pi c\tau_0/\lambda$ . We can identify three main contributions to this intrinsic  $Q$  factor:

$$\frac{1}{Q_0} = \frac{1}{Q_{\text{rad}}} + \frac{1}{Q_{\text{mat}}} + \frac{1}{Q_s}. \quad (19)$$

The first term  $Q_{\text{rad}}$  refers to curvature losses, for our values of  $\ell$ , with  $n = 1$  we obtain  $Q_{\text{rad}} > 10^{34}$  [48]. Its contribution to  $Q_0$  is totally negligible.  $Q_{\text{mat}}$  is associated with absorption and bulk Rayleigh backscattering. In silica at  $\lambda = 1.55 \mu\text{m}$  the attenuation coefficient is  $\alpha = 0.17 \text{ dB/km}$ , which leads to  $Q_{\text{mat}} = 1.5 \times 10^{11}$  considering that

$$Q_{\text{mat}} = \frac{4.3 \times 10^3}{\alpha} \times \frac{2\pi N}{\lambda}. \quad (20)$$

Considering Rayleigh backscattering as the only contribution to  $Q_{\text{mat}}$ , we can write [33]

$$Q_{\text{mat}} = \frac{3N\lambda^3}{4\pi^2 \rho_{sc}\bar{\alpha}^2}. \quad (21)$$

With the value of  $\rho_{sc}\bar{\alpha}^2$  we have used for the frequency splitting estimation, we obtain  $Q_{\text{mat}} = 2 \times 10^{11}$  which shows that this assumption is consistent with silica attenuation. The intrinsic  $Q$  factors  $Q_0$  measured in the present work range from  $1.4 \times 10^8$  to  $2.1 \times 10^8$ . Considering Eq. (10), with our values we had to keep  $\tau_e \gg \tau_0$  in order to observe the coupled-cavity ringing phenomenon. We have  $Q_{\text{rad}} \gg Q_0$  and  $Q_{\text{mat}} \gg Q_0$ , thus  $Q_0$  seems to be limited by surface effects characterized by  $Q_s$ . If  $Q_0$  was limited by other stronger

surface scattering processes we would have found some larger frequency splittings [35,41]. Consequently we can think that in our experiments, the intrinsic  $Q$  factor is limited by surface absorption. In the infrared (here  $\lambda = 1.55 \mu\text{m}$ ) this absorption is attributed to chemisorption of  $\text{OH}^-$  ions and water on the surface of the sphere [2,51]. In this regime the  $Q_0$  obtained here is consistent with other experiments carried out with silica WGM resonators [41].

(c) *Interests of the method.* In Ref. [28], the authors have shown that the ringdown technique allows one to circumvent the drawbacks of usual stationary characterizations of very high- $Q$  WGM resonators [i.e., (i) the use of highly stabilized lasers, and (ii) detrimental nonlinear effects such as Raman scattering or thermal drift are enhanced due to the large buildup factor of the microresonator]. Our results show that by taking into account the interaction between two counterpropagating modes, this method can be extended to WGM doublets which was not possible using a straightforward analysis of the ringdown signal as reported in Ref. [28]. From the beating between the input and output fields, the proposed method intrinsically gives an accurate evaluation of the frequency speed which avoids any calibration. As is the case for single resonators, the method gives a direct measurement of  $Q_0$  without any assumptions [29]. We can also note that this method gives the value of  $\gamma$  instead of  $\delta_C$  even in the case of weak values of frequency splitting. Furthermore, the proposed method is strongly sensitive and would allow very low values of  $1/(2\pi\gamma)$  of the same magnitude as the intrinsic linewidth of the resonator to be measured. The latest property could be used in single nanoparticle sizing based on frequency splitting in a high- $Q$  microresonator as proposed by J. Zhu *et al.* in Ref. [42].

#### IV. CONCLUSION

We have theoretically studied the ringing phenomenon in coupled cavities and applied it to the particular case of modal coupling. We have presented calculations of the transient profile of a coupled resonator transmission signal obtained with a linearly swept excitation frequency. From an experimental point of view, the analysis of the time domain profile allows one to fully and accurately describe the split resonances of high- $Q$  WGM resonators without (i) any calibration of the frequency sweeping speed and (ii) the use of highly stabilized lasers. The method has been applied to the modal coupling characterization in silica microspheres. The proposed simple method is expected to find some applications in the characterization of ultra-high- $Q$ -factor microresonators. It could be generalized in order to study lift of degeneracy whose origin comes from other physical mechanisms such as additional microresonator coupling and single emitter or nanoparticle scattering [42]. Finally, it could find some applications in quantum optics since it has recently shown that a thorough analysis of frequency splitting under strong backscattering can be used to measure the Purcell factor [41].

#### ACKNOWLEDGMENTS

This work was supported by the Centre National d'Études Spatiales through convention No. 60281/00.

- [1] K. J. Vahala, *Nature (London)* **424**, 839 (2003).
- [2] A. B. Matsko and V. S. Ilchenko, *IEEE J. Sel. Top. Quantum Electron.* **12**, 3 (2006).
- [3] V. S. Ilchenko and A. B. Matsko, *IEEE J. Sel. Top. Quantum Electron.* **12**, 15 (2006).
- [4] T. A. Ibrahim, K. Amarnath, L. C. Kuo, R. Grover, V. Van, and P.-T. Ho, *Opt. Lett.* **29**, 2779 (2004).
- [5] T. J. Kippenberg, S. M. Spillane, and K. J. Vahala, *Phys. Rev. Lett.* **93**, 083904 (2004).
- [6] V. S. Ilchenko, A. A. Savchenkov, A. B. Matsko, and L. Maleki, *Phys. Rev. Lett.* **92**, 043903 (2004).
- [7] V. V. Vasilev, V. L. Velichansky, M. L. Gorodetsky, V. S. Ilchenko, L. Hollberg, and A. V. Yarovitski, *Quantum Electron.* **26**, 657 (1996).
- [8] F. Lissillour, R. Gabet, P. Féron, P. Besnard, and G. Stéphan, *Europhys. Lett.* **55**, 499 (2001).
- [9] G. Lenz, B. J. Eggleton, C. K. Madsen, and R. E. Slusher, *IEEE J. Quantum Electron.* **37**, 525 (2001).
- [10] Q. Xu, P. Dong, and M. Lipson, *Nat. Phys.* **3**, 406 (2007).
- [11] S. Arnold, M. Khoshshima, I. Teraoka, S. Holler, and F. Vollmer, *Opt. Lett.* **28**, 272 (2003).
- [12] T. Aoki, B. Dayan, E. Wilcut, W. P. Bowen, A. S. Parkins, T. J. Kippenberg, K. J. Vahala, and H. J. Kimble, *Nature (London)* **443**, 671 (2006).
- [13] B. E. Little, S. T. Chu, H. A. Haus, J. Foresi, and J.-P. Laine, *IEEE J. Lightwave Technol.* **15**, 998 (1997).
- [14] Y. Dumeige, L. Ghiša, and P. Féron, *Opt. Lett.* **31**, 2187 (2006).
- [15] Y. Xu, R. K. Lee, and A. Yariv, *J. Opt. Soc. Am. B* **17**, 387 (2000).
- [16] Y. Dumeige, *Opt. Lett.* **32**, 3438 (2007).
- [17] A. Melloni, F. Morichetti, and M. Martinelli, *J. Opt. Soc. Am. B* **25**, C87 (2008).
- [18] Y. Dumeige and P. Féron, *Phys. Rev. E* **72**, 066609 (2005).
- [19] A. Yariv, Y. Xu, R. K. Lee, and A. Scherer, *Opt. Lett.* **24**, 711 (1999).
- [20] J. E. Heebner, R. W. Boyd, and Q.-H. Park, *J. Opt. Soc. Am. B* **19**, 722 (2002).
- [21] J. B. Khurgin, *Opt. Lett.* **30**, 513 (2005).
- [22] Y. Dumeige, *Europhys. Lett.* **86**, 14003 (2009).
- [23] H. J. Schmitt and H. Zimmer, *IEEE Trans. Microwave Theory Tech.* **14**, 206 (1966).
- [24] Z. K. Ioannidis, P. M. Radmore, and I. P. Giles, *Opt. Lett.* **13**, 422 (1988).
- [25] J. Poirson, F. Bretenaker, M. Vallet, and A. Le Floch, *J. Opt. Soc. Am. B* **14**, 2811 (1997).
- [26] L. Matone, M. Barsuglia, F. Bondu, F. Cavalier, H. Heitmann, and N. Man, *Phys. Lett. A* **271**, 314 (2000).
- [27] I. S. Grudin, V. S. Ilchenko, and L. Maleki, *Phys. Rev. A* **74**, 063806 (2006).
- [28] A. A. Savchenkov, A. B. Matsko, V. S. Ilchenko, and L. Maleki, *Opt. Express* **15**, 6768 (2007).
- [29] Y. Dumeige, S. Trebaol, L. Ghiša, T. K. N. Nguyễn, H. Tavernier, and P. Féron, *J. Opt. Soc. Am. B* **25**, 2073 (2008).
- [30] C. Dong, C. Zou, J. Cui, Y. Yang, Z. Han, and G. Guo, *Chin. Opt. Lett.* **7**, 299 (2009).
- [31] W. Yang, A. Joshi, and M. Xiao, *Opt. Lett.* **29**, 2133 (2004).
- [32] Y. Dumeige, S. Trebaol, and P. Féron, *Phys. Rev. A* **79**, 013832 (2009).
- [33] D. S. Weiss, V. Sandoghdar, J. Hare, V. Lefèvre-Seguin, J.-M. Raimond, and S. Haroche, *Opt. Lett.* **20**, 1835 (1995).
- [34] M. L. Gorodetsky, A. D. Pryamikov, and V. S. Ilchenko, *J. Opt. Soc. Am. B* **17**, 1051 (2000).
- [35] T. J. Kippenberg, S. M. Spillane, and K. J. Vahala, *Opt. Lett.* **27**, 1669 (2002).
- [36] M. Borselli, K. Srinivasan, P. E. Barclay, and O. Painter, *Appl. Phys. Lett.* **85**, 3693 (2004).
- [37] M. Mohageg, A. Savchenkov, and L. Maleki, *Opt. Lett.* **32**, 2574 (2007).
- [38] X.-W. Wu, C.-L. Zou, J.-M. Cui, Y. Yang, Z.-Fu Han, and G.-C. Guo, *J. Phys. B: At. Mol. Opt. Phys.* **42**, 085401 (2009).
- [39] K. Srinivasan and O. Painter, *Phys. Rev. A* **75**, 023814 (2007).
- [40] A. Mazzei, S. Götzinger, L. de S. Menezes, G. Zumofen, O. Benson, and V. Sandoghdar, *Phys. Rev. Lett.* **99**, 173603 (2007).
- [41] T. J. Kippenberg, A. L. Tchebotareva, J. Kalkman, A. Polman, and K. J. Vahala, *Phys. Rev. Lett.* **103**, 027406 (2009).
- [42] J. Zhu, S. K. Ozdemir, Y.-F. Xiao, L. Li, L. He, D.-R. Chen, and L. Yang, *Nature Photon.* **4**, 46 (2010).
- [43] K. Kieu and M. Mansuripur, *Opt. Lett.* **31**, 3568 (2006).
- [44] K. Kieu and M. Mansuripur, *Opt. Lett.* **32**, 244 (2007).
- [45] H. A. Haus, *Waves and Fields in Optoelectronics* (Prentice-Hall, Upper Saddle River, 1984).
- [46] J. C. Knight, G. Cheung, F. Jacques, and T. A. Birks, *Opt. Lett.* **22**, 1129 (1997).
- [47] A. A. Savchenkov, V. S. Ilchenko, A. B. Matsko, and L. Maleki, *Phys. Rev. A* **70**, 051804(R) (2004).
- [48] F. Treussart, Ph.D thesis, Université Pierre et Marie Curie, France, 1997.
- [49] C. C. Lam, P. T. Leung, and K. Young, *J. Opt. Soc. Am. B* **9**, 1585 (1992).
- [50] A. Chiasera, Y. Dumeige, P. Féron, M. Ferrari, Y. Jestin, G. Nunzi Conti, S. Pelli, S. Soria, and G. C. Righini, *Laser & Photon. Rev.* (2009) [online] doi:10.1002/lpor.200910016.
- [51] M. L. Gorodetsky, A. A. Savchenkov, and V. S. Ilchenko, *Opt. Lett.* **21**, 453 (1996).